CRACK PROPAGATION IN HETEROGENEOUS BRITTLE MATERIALS : TRAJECTORY AND PROPAGATION THRESHOLD

M. Lebihain[a,b], J-B. Leblond[a], L. Ponson[a], M. Bornert[b]
[a] Institut Jean le Rond d'Alembert (SU/CNRS) - mail : lebihain@dalembert.upmc.fr
[b] Laboratoire Navier (ENPC/IFSTTAR/CNRS)

Keywords : heterogeneous materials, brittle fracture, crack trajectory, surface roughness, effective toughness, quantitative fractography

Abstract

A good understanding of a material failure behavior is a prerequisite to make reliable predictions on the resistance and lifetime of structures or to design meta-materials with increased fracture properties. This work aims at understanding the effect of toughness discontinuities on both crack trajectory and material toughness in brittle solids. A 3D first-order model has been designed to describe the interaction between a semi-infinite crack with spherical defects through a $(G - G_c)_{max}$ criterion. Its numerical efficiency allows simulations for very large distributions ($\sim$ 1M inclusions) in a very short computational time ($\sim$ 1 hour), thus paving the way to tackle the difficult questions of homogenization in brittle fracture or fracture surface roughness.

1 Introduction

Heterogeneous materials are all around us, be it by choice (e.g. concrete, composite) or by mistake (e.g. welding defects, quenching of a workpiece). With the recent emergence of new manufacturing techniques (e.g. 3D printing) and the rise in importance of social and environmental concerns (e.g. recycling plastic waste in concrete), the number of meta-materials will flourish, thus leading to a greater focus on the failure of heterogeneous materials.

In order to make reliable forecasts on the resistance and lifetime of structures, there need to be criteria, which allow a good prediction on the crack trajectory and the threshold at which this propagation happens, also called material toughness. These criteria have been developed for homogeneous materials and display a good match with experiments. Yet, when it comes to the case of heterogeneous materials, classical methods such as linear elastic fracture mechanics (LEFM) are unable to predict properly the role played by small-scale defects on the macroscopic behavior of solids. Two main approaches have been developed in order to tackle the problem of crack propagation in brittle materials displaying toughness discontinuities. The first one consists in applying perturbative approaches based on LEFM perturbative formulae established successively by Gao and Rice [1] and Movchan, Gao and Willis [5], considering then crack propagation as a depinning transition. Most papers focus on coplanar propagation of a crack in a brittle material displaying toughness discontinuities [4, 2, 3] but some work extend this model to full 3D simulations [6]. This framework allows fast computation on large scales but material disorder is modeled as a stochastic noise and fundamental interactions between a crack and defects are thus ignored. The second approach is quite the opposite since it aims at describing accurately the interaction between a crack and a given microstructure through finite element simulations with phase field or cohesive zone models [9]. It is then necessary to mesh all the defects and their interface with the surrounding matrix at a fine resolution, resulting in a huge computational cost. The studies are then often restricted in 2D or display only few defects in 3D.

Our approach aims at describing with a pertubative approach the fundamental interactions of a crack with tougher defects through a crossing/by-pass transition, which is observed experimentally on natural materials such as clay (Fig. 1). We will thus benefit from the high computational performances of the perturbation based models but still grasp the effect of individual defect material or geometrical properties. Based on 3D pertubations formulae coupled with Amestoy-Leblond's equations, this model will allow us to tackle the two main points of interest in fracture mechanics : the crack trajectory and the associated fracture surface, and the propagation threshold of such disordered materials, the effective toughness.

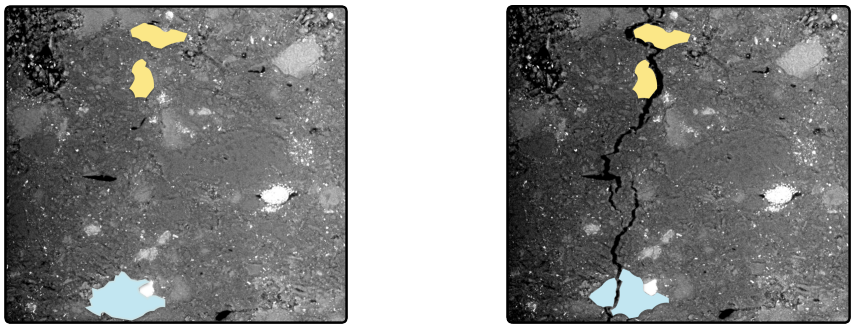

(a) Sane clay (b) Fractured clay

FIGURE 1 – Sane and fractured clay with by-passed (in beige) and crossed (in blue) inclusions (courtesy of M. Bornert)

2 Theoretical model and numerical implementation

Brittle fracture is based on an energy balance between the elastic restitution rate (ERR), G, energy stored in the crack tip and released during crack propagation, and the material toughness G_c, resistance to fracture. In order to model the propagation of a single crack front in a given heterogeneous brittle medium, our model will need three main ingredients detailed below :

1. the heterogeneous toughness map G_c at each point in our medium ;
2. the energetic configuration G of each point of the crack front for any configuration possible ;
3. a propagation criterion, which will connect G and G_c to predict how the crack will progress.

2.1 Microstructure

Our medium is made of a heterogeneous material constituted by two phases : a homogeneous matrix and spherical inclusions. The inclusions are considered isotropically distributed and their diameters follow a monodisperse or polydisperse distribution characterized by its mean d and its standard deviation σ_d.

We suppose that both the matrix and the inclusions are isotropically linear elastic and share the same elastic properties (E, ν). And we assume that all the dissipative processes located in the vicinity of the crack tip (e.g. bond breaking, plasticity, microcracking) are confined in a process zone much smaller than the heterogeneity size d. Under this hypothesis, both phases are brittle but they differ in their fracture properties : the inclusions may be a little tougher or/and weakly bonded to the matrix. These properties are characterized by their inner toughness contrast c_s^{in} and their interfacial toughness c_s^{out}, defined as :

$$\begin{aligned} G_c^{inclusion} &= G_c^{matrix}\left(1 + c_s^{in}\right), \ \left|c_s^{in}\right| \ll 1 \\ G_c^{interface} &= G_c^{matrix}\left(1 + c_s^{out}\right), \ c_s^{out} < 0 \text{ and } \left|c_s^{out}\right| \ll 1 \end{aligned} \tag{1}$$

where $G_c^{matrix} = \dfrac{1-\nu^2}{E} K_{I,c}^2$ is the matrix toughness, $G_c^{inclusion}$, the inclusion inner toughness and $G_c^{interface}$, the toughness of the interface, as depicted in Fig. 3.

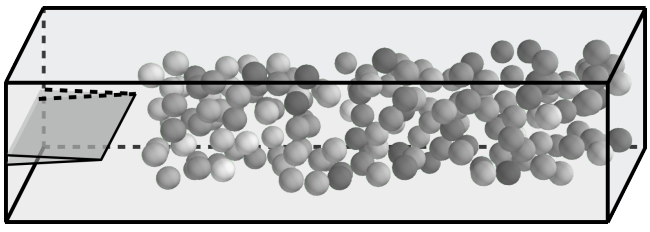

FIGURE 2 – Semi-infinite crack facing monodisperse inclusions distribution with varying inner toughness contrast (in grey level)

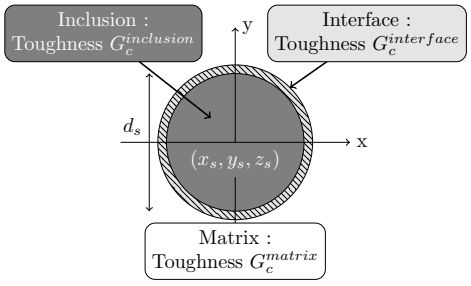

FIGURE 3 – A weakly-bonded tougher inclusion I_s embedded in the matrix and its properties

2.2 Perturbative approach for SIF calculation

We consider an semi-infinite tensile crack embedded in an infinite periodic medium. In the following, we adopt the usual convention of linear elastic fracture mechanics and note x, the direction of crack propagation, y, the direction of tensile loading, z, the direction parallel to the crack front Γ, and L_z, the period in the z-direction. At a given time t, the position of the crack front from the origin is noted $x\left(t\right)$. (Fig. 4).

2.2.1 Loading and sample geometry

This material is loaded in tensile mode (Mode I) with prescribed displacement. Since, we want to study the effect of loading conditions and sample geometry through as few parameters as possible, we follow the theoretical framework developed for coplanar propagation [3]. In that case, we can write at the first order :

$$G^{ref}\left(t\right) = G_0\left(1 + \frac{v_m t - x\left(t\right)}{\mathcal{L}}\right) \tag{2}$$

where G_0 is the initial loading, $\mathcal{L}$, the structural length related to the sample geometry and v_m, crack mean velocity related both to the loading and sample geometry.

2.2.2 SIF first-order estimation

In the absence of heterogeneities and under the tensile loading described above, the semi-infinite crack would undergo a stable coplanar propagation and the crack front Γ will remain straight in the direction z. But the material disorder will distort the crack line both in-plane (e.g. crack pinning, crack bridging) [4, 2] and out-of-plane (e.g. crack deflection or defect by-pass, the mechanism we aim at modeling) [6]. In the following, we will note $f_x\left(z,t\right)$, the in-plane perturbation of the crack front and $f_y\left(z,t\right)$, the out-of-plane perturbation. These perturbations are defined from a reference crack configuration which is a semi-infinite plane crack in $x\left(t\right)$ (Fig. 4).

Thanks to the work of Gao and Rice for the in-plane situation [1] and Movchan, Gao and Willis for the out-of-plane problem [5], we are able to link those geometrical perturbations f_x and f_y to stress intensity factors (SIF) perturbations $\left(\delta K_i\right)_{i\in\{I,II,III\}}$. Under standard assumptions [3] :

$$\begin{cases} \dfrac{\delta K_I\left(z,t\right)}{K_I^{ref}\left(t\right)} = -\dfrac{1}{2\mathcal{L}} f_x\left(z,t\right) - \dfrac{1}{2\pi}\,\mathrm{PV}\int_{-\infty}^{+\infty} \dfrac{f_x\left(z,t\right) - f_x\left(z',t\right)}{\left(z-z'\right)^2}\,dz' \\ \dfrac{\delta K_{II}\left(z,t\right)}{K_I^{ref}\left(t\right)} = \dfrac{1}{2}\dfrac{\partial f_y}{\partial x}\left(z,t\right) + \dfrac{2-3\nu}{2-\nu}\dfrac{1}{2\pi}\,\mathrm{PV}\int_{-\infty}^{+\infty} \dfrac{f_x\left(z,t\right) - f_x\left(z',t\right)}{\left(z-z'\right)^2}\,dz' \\ \dfrac{\delta K_{III}\left(z,t\right)}{K_I^{ref}\left(t\right)} = -\dfrac{2\left(1-\nu\right)^2}{2-\nu}\dfrac{\partial f_y}{\partial z}\left(z,t\right) \end{cases} \tag{3}$$

where the principal value (PV) ensures the convergence of the integral.

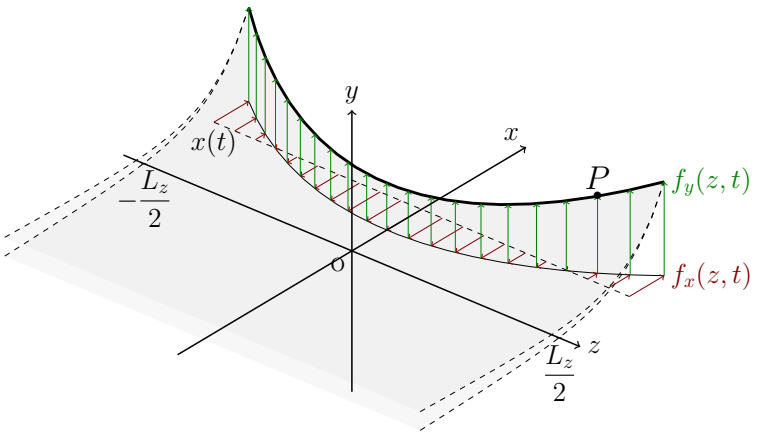

FIGURE 4 – Perturbated crack with $f_x\left(z,t\right)$, in-plane perturbations along the crack front (in thick black), and $f_y\left(z,t\right)$, out-of-plane one, around a semi-infinite reference plane crack in $x\left(t\right)$

2.3 Propagation criterion

2.3.1 Kinetic law

A linearization of Griffith's criterion around the mean crack velocity v_m leads to the following kinetic law, which has shown good agreement with experiments [3] :

$$G = G_c(v) \Leftrightarrow v = \left[v_m + v_0 \frac{G - G_c(v_m)}{G_c(v_m)} \right]^+ \tag{4}$$

where v_0 is a material characteristic velocity and $[\cdot]^+$ is the positive part function.

2.3.2 Direction criterion - $(G - G_c)_{max}$

Standard direction criteria, such as the principle of local symetry (PLS) or the maximum energy release rate criterion (MERR), already exist in homogeneous LEFM but we here have to deal with toughness heterogeneities and especially discontinuities. The PLS cannot be used since it is based on isotropy considerations which are violated in our case with an heterogeneous toughness distribution along the propagation direction θ (Fig. 6.a). As for the MERR, it does not take into account this heterogeneous distribution either but it can naturally be extended into the following condition [9, 8] :

$$\text{Propagation at } \theta \text{ such as } (G - G_c)(\theta) \text{ is globally maximal} \tag{5}$$

Let us consider a crack which just has just landed in P on an inclusion with an attack angle θ_{ini} at a landing height $y_{landing} = (y_p - y_s)$ thus facing a discontinuity with a tangent angle θ_{tan} as depicted in Fig. 5. The distribution $G_c(\theta)$ is given by the microstructure and the distribution of G is extracted from Irwin's formulae coupled with Amestoy and Leblond's equations [7] :

$$\begin{cases} K_I(\theta) = F_{I,I}(\theta - \theta_{ini}) K_I^p + F_{I,II}(\theta - \theta_{ini}) K_{II}^p \\ K_{II}(\theta) = F_{II,I}(\theta - \theta_{ini}) K_I^p + F_{II,II}(\theta - \theta_{ini}) K_{II}^p \\ K_{III}(\theta) = F_{III,III}(\theta - \theta_{ini}) K_{III}^p \end{cases} \tag{6}$$

where K_I^p, K_{II}^p and K_{III}^p are given via perturbative formulae (Eq. (6)). By subtracting them, we get the distribution of $(G - G_c)$ in each direction θ (Fig. 6.c). The crack will propagate in the direction where $(G - G_c)$ is maximal as soon as Griffith's criterion $(G - G_c) \geq 0$ is satisfied.

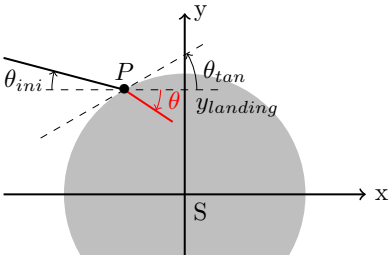

FIGURE 5 – A crack landing on an inclusion

When a point P is propagating along the interface, we apply the same criterion thus allowing the crack to stay on the interface, stop the by-pass and cross the inclusion or leave the interface and go back to the matrix. Finally, when a point P is either in the matrix or crossing an inclusion, $G_c(\theta)$ is homogeneous and we choose to keep the $(G - G_c)_{max}$ criterion which is then equivalent to the MERR.

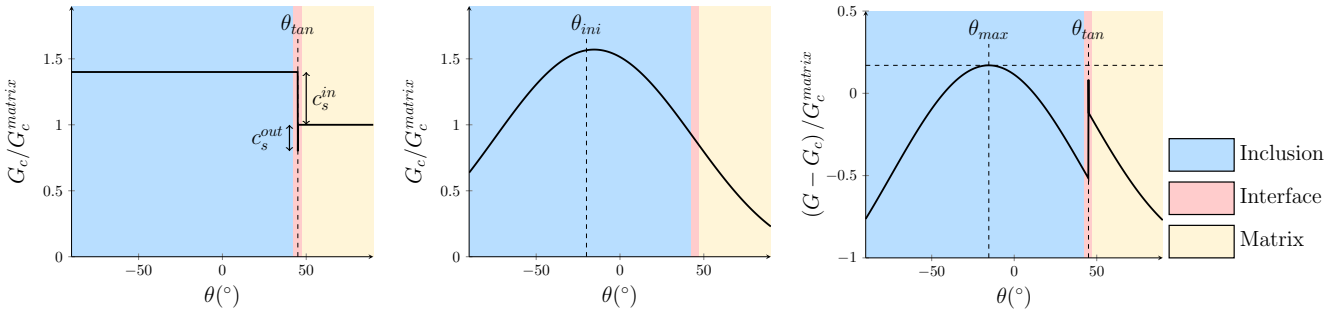

(a) $G_c(\theta)$ (b) $G(\theta)$ (c) $(G - G_c)(\theta)$

FIGURE 6 – Angle distribution of G_c, G and $(G - G_c)$

2.4 2D theoretical by-pass/crossing phase diagram

Thanks to this criterion, we understand that the by-pass/crossing mechanism is an energetic competition between how it will cost to kink and by-pass the inclusion versus how tough the inclusion is. Thus it will strongly depend on θ_{tan} or equivalently $y_{landing}$ and c_s^{in}, c_s^{out}, the inner and interfacial contrasts of the inclusion. This phase transition can be quantitatively explained with Amestoy and Leblond's formulae. Indeed, in the limit case where $(G - G_c)(\theta_{tan}) = (G - G_c)(0°)$, assuming $K_{II}^p = K_{III}^p = 0$ and $\theta_{ini} = 0$, we get the following relationship :

$$F_{I,I}(\theta_{tan})^2 + F_{II,I}(\theta_{tan})^2 = \frac{1 + c_s^{out}}{1 + c_s^{in}} \tag{7}$$

If we assume that the matrix and the inclusion are perfectly bonded i.e. $c_s^{out} = 0$, we can plot the diagram in Fig. 7 from Eq. (7). We see that, if the crack land on the top of the inclusion, it will not by-pass it downwards and is more and more likely to by-pass it upwards as the inner contrast increase. Moreover, there is critical inner contrast $c_{crit}^{in} \simeq 2.854$ above which every inclusion is by-passed no matter its contrast. These 2D-diagrams have been shown to depict fairly well the phase diagram for a spherical defect geometry, which is the scope of the present study, but can be invalidated for different geometry such as ellipsoidal inclusions.

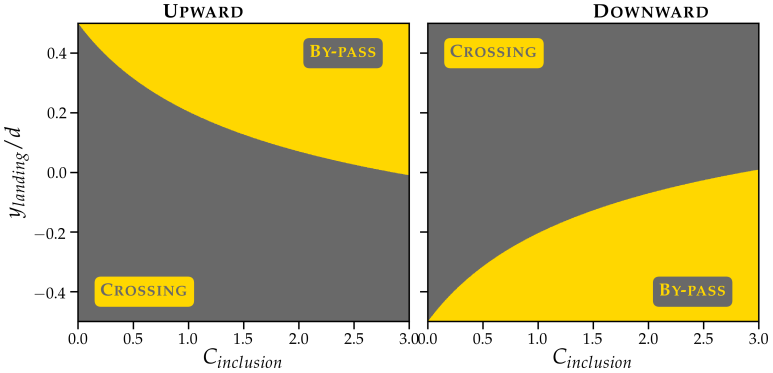

FIGURE 7 – By-pass (in yellow) / crossing (in grey) phase diagram for a crack landing at a height $y_{landing}$ on a inclusion of contrast $c_{inclusion}$

2.5 Numerical implementation

The following model has been implemented in C with an explicit scheme. The crack front is discretized in N equidistant points. At a time t, we compute efficiently the perturbated SIF $(\delta K_i)_i$ from Eq. (3) with an direct and inverse FFT, taking advantage of the simple form of these equations in the Fourier space. From Eq. (4) and (5), we deduce the full speed vector (norm and direction) in each point of the crack front and make each point of the crack front advance with a step Δt_{step}, thanks to a global convergence criterion and an acceleration procedure. The geometrical configuration of the crack front is updated and the procedure goes on. This algorithm allows fast computation (1 hour) on a large scale (1M inclusions in the medium and interaction with around 200k) with fine resolution (32 points per diameter) Fig (8.a) and simulate the fundamental interaction between a crack front and toughness discontinuities through a by-pass/crossing mechanism Fig (8.b).

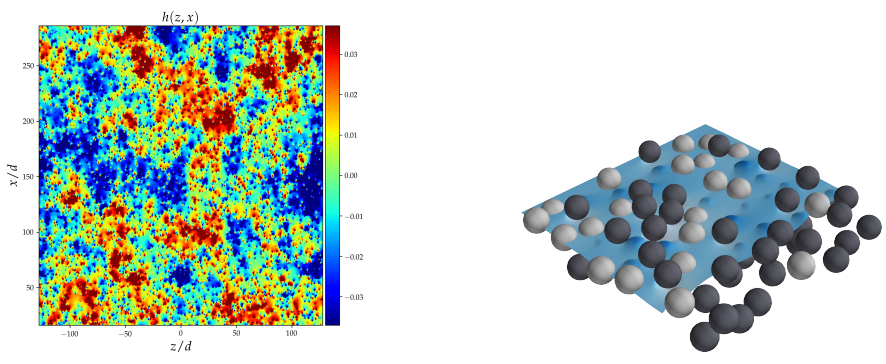

(a) (b)

FIGURE 8 – Fracture surface resulting from the interaction between the crack front and 200k inclusions (a) and propagation in a smaller medium with by-passed inclusions (in black) and crossed one (in grey)

3 Effective toughness and quantitative fractography

3.1 Effective toughness of brittle materials

The numerical method presented above allows us to track in real time the position of each point of the crack front but also other physical variables such as the local ERR G. Thus, we can discretize our medium in a regular (x0z) grid $(z_{i,j}, x_{i,j})_{i,j}$ with a spatial step $d\ell$ (Fig 9.a). By sticking to Griffith's definition of the material toughness, we define the local effective toughness on each square of the grid as the energy required to crack this fundamental surface :

$$G_{c\,i,j}^{eff} = \frac{1}{d\ell^2} \int_{t_{i,j}^{in}}^{t_{i,j}^{out}} \int_{z_{i,j}-d\ell/2.}^{z_{i,j}+d\ell/2.} G\left(z,t\right) v\left(z,t\right) dzdt \tag{8}$$

where $t_{i,j}^{in}, t_{i,j}^{out}$ are the starting and exit time defined in Fig 9.a.

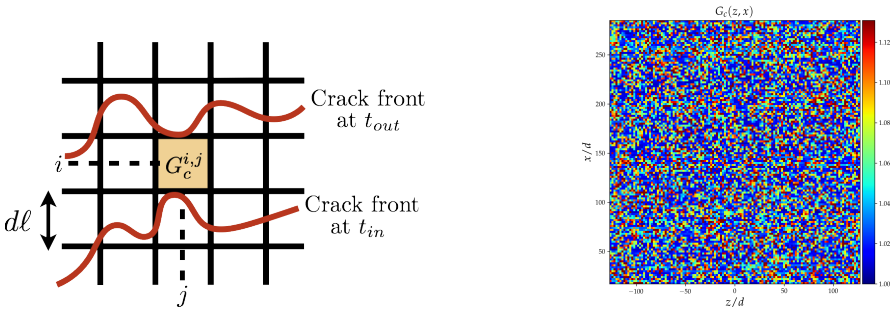

(a) (b)

FIGURE 9 – Definition of the local effective toughness on a grid and example of a toughness map for $d\ell = d$, mean defect size

In the following, we will take G_c^{eff} as the mean on the whole grid $< G_{c\,i,j}^{eff} >$. By running multiple simulations on 5 different microstructures for various defect inner contrast and inclusion densities, we can study the variation of G_c^{eff} as the inclusions get tougher and their distribution denser.

The results are plotted in Fig 10 and are compared to coplanar propagation results. We can notice two main regimes : a first one at low contrast where the effective toughness is increasing with the toughness contrast no matter the inclusion density. In this regime, there are fewer and fewer crossed inclusions (Fig 10.(c)) but their inner contrast is increasing so the overall toughness increase in spite of the local toughness decrease due to the by-pass of the toughest inclusions. Then we can observe a maximum, due to this competition between toughening (crossing) and softening (by-pass) effects. It is followed by a plateau regime where every inclusion is by-passed by the crack.

The comparison between the coplanar toughness and 3D effective toughness show how crucial it is to prevent any by-pass of the inclusion if we want to design tougher material. Thus, by playing on the geometry of our defect and choosing them for example concave instead of convex, we could achieve greater reinforcement.

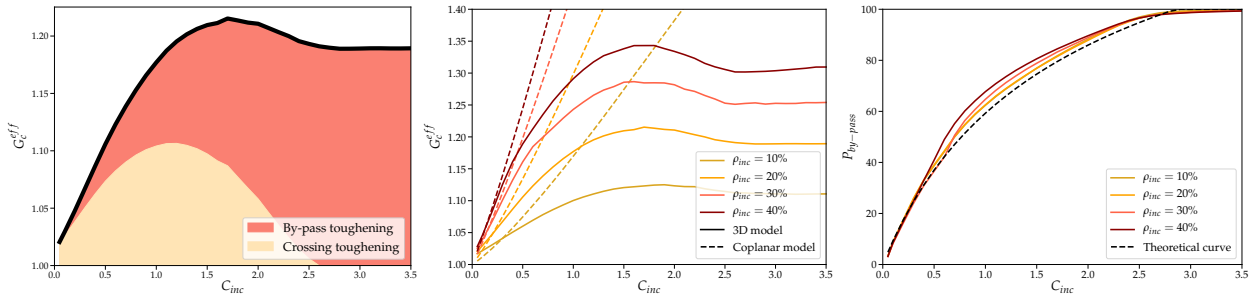

(a) (b) (c)

FIGURE 10 – G_c^{eff} as a function of toughness contrast c_{inc} for an inclusion density $\rho_{inc} = 20\%$ with contributions (a), for multiple density with a comparison to coplanar case (b) and by-pass probability (c)

3.2 Quantitative fractography

Fracture surfaces, as a persistent signature of crack propagation, may contain detailed information on the failure mechanisms. The goal of quantitative fractography is to extract failure information from the fracture surfaces statistical properties. Our model meet all the mandatory criteria to extend classical quantitative fractography method to brittle materials since it can produce fracture surfaces and toughness maps through the model described above.

Following the method of Vernede et al. [10], we define a slope operator $\omega = \frac{1}{2}\log\left[\left\langle \left(h\left(\boldsymbol{x}+\delta\boldsymbol{x}\right)-h\left(\boldsymbol{x}\right)\right)^2\right\rangle_{|\delta\boldsymbol{x}|=\varepsilon}\right]$, which put in light the zone of intense fracture processes. In quasi-brittle and ductile materials, its correlations display a logarithmic decrease up to a correlation length ξ, which can be linked to the toughness of the material G_c. When we apply the same operator to our fracture surfaces (Fig 11.a and b), we get an ω-map close to the one observed on ceramics [10] and it displays the same logarithmic decrease, allowing us to define an internal length ξ respective to the inclusion size d.

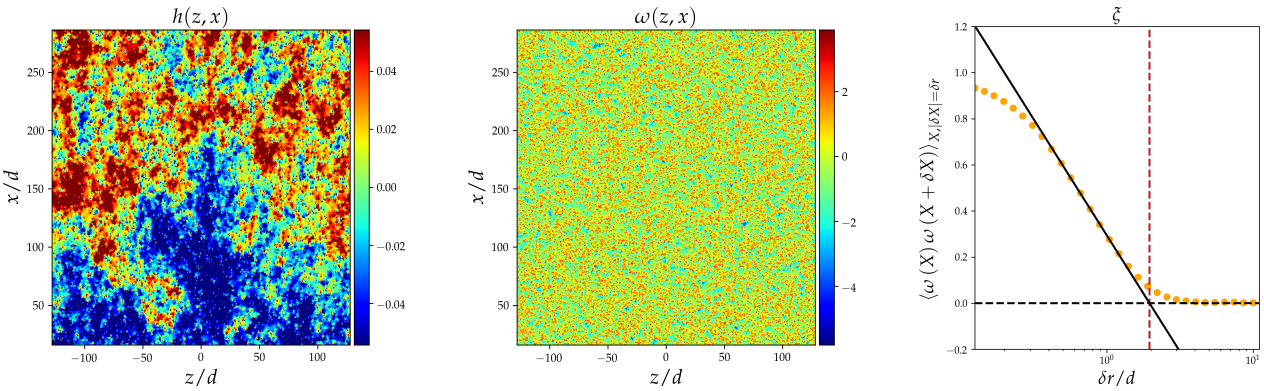

(a) (b) (c)

FIGURE 11 – Fracture surface extracted from our simulations with the associated ω-map and its correlator exhibiting a correlation length ξ

This length has be found to be the characteristic length between two by-passed inclusions since it scales numerically as $\xi \sim d(1+\alpha P_{by-pass}^{-\frac{1}{2}})$ (Fig 12.a and b), just as the intensity of a process of density $P_{by-pass}$, probability to by-pass an inclusion. This length is naturally linked to the effective toughness and can be a measurement of the intensity and density of defects in a brittle materials. It is also a variable to be played on in order to design materials with greater fracture properties.

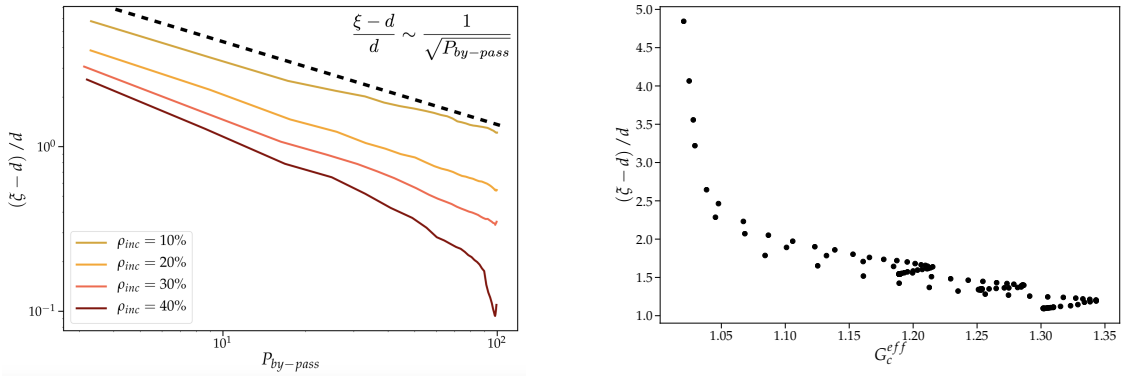

(a) (b)

FIGURE 12 – Fracture surface extracted from our simulations with the associated ω-map and its correlator exhibiting a correlation length ξ

4 Conclusion and perspectives

By coupling perturbative methods with Amestoy and Leblond's formulae, we designed a theoretical model capable of describe crack propagation in an heterogeneous brittle medium displaying toughness discontinuities. The perturbative approach associated with innovative acceleration strategy allows fast simulations on large scale with a fine description of the fundamental interaction of a crack and inclusions, through a crossing/by-pass energetic transition. This performances, unreachable through standard simulation methods such as FEM, open the way to tackle the difficult issue of homogenization in brittle fracture. The effective toughness of disordered materials has been predicted, underlining the softening effect of the by-pass mechanism and giving clues to design tougher materials. Finally, signature of fracture properties on fracture have been highlighted through the extension of new quantitative fractography methods to brittle fracture and the physical explanation of the internal length ξ, extracted from fracture surface statistical properties.

Experimental validation of this theoretical and numerical have still to be produced. In order to do this, we designed disordered materials by printing heterogeneous TDCB samples through additive manufacturing techniques with polymers (Fig 13). At this time, we proved that the crack propagation is indeed toughness driven and not elastically driven (with crack denucleation and renucleation) as in our model. These experiments have been conducted on striped samples and analyzed through DIC techniques (Fig 13.a). The next step is to test disordered samples with spherical inclusions under tensile conditions (Fig 13.b), thus allowing a direct comparison between theory, simulations and experiments.

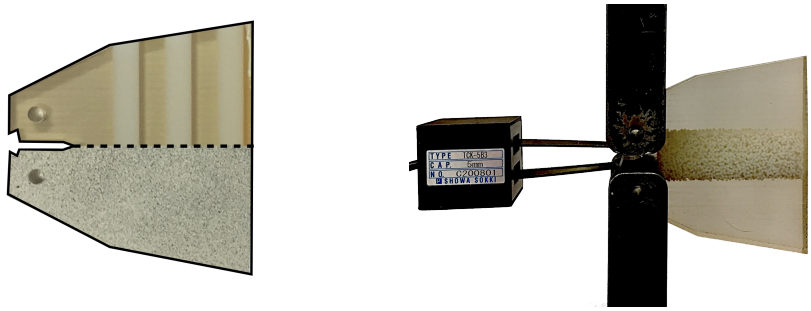

(a) (b)

FIGURE 13 – TDCB samples with striped inclusions and DIC pattern (a) and samples with spherical distribution of inclusions as modeled above (b)

Références

[1] H. Gao and J.R. Rice Shear Stress Intensity Factors for a Planar Crack With Slightly Curved Front *International Journal of Solids and Structures*, 53 (1986) 774–778.

[2] A.F. Bower and M.Õrtiz Solution of three-dimensional crack problems by a finite perturbation method *Journal of the Mechanics and Physics of Solids*, 38 (1990) 443–480.

[3] L. Ponson Statistical aspects in crack growth phenomena : how the fluctuations reveal the failure mechanisms *International Journal of Fracture*, 201 (2016) 11–27.

[4] H. Gao and J.R. Rice A First-Order Perturbation Analysis of Crack Trapping by Arrays of Obstacles *Journal of Applied Mechanics*, 56 (1989) 828–836.

[5] H. Gao and J.R. Rice On perturbations of plane cracks *International Journal of Solids and Structures*, 26 (1998) 3419–3453.

[6] S. Ramanathan and D. Ertaz and D.S. Fisher Quasistatic Crack Propagation in Heterogeneous Media *Physical Review Letters*, 79 (1997) 873–876.

[7] J.B. Leblond Crack paths in three-dimensional elastic solids. i : two-term expansion of the stress intensity factors *International Journal of Solids and Structures*, 36 (1999) 79–103.

[8] A. Chambolle and G.A. Francfort and J.J Marigo When and how do cracks propagate ? *Journal of the Mechanics and Physics of Solids*, 57 (2009) 1614–1622.

[9] V. Hakim and A. Karma Crack Path Prediction in Anisotropic Brittle Materials *Journal of the Mechanics and Physics of Solids*, 95 (2005)

[10] S. Vernède and L. Ponson and J.P. Bouchaud Turbulent Fracture Surfaces : A Footprint of Damage Percolation ? *Physical Review Letters*, 114 (2015)